J Ginseng Res 41 (2017) 392–402

Contents lists available at ScienceDirect

Journal of Ginseng Research

journal homepage: http://www.ginsengres.org

Research article

20S-Protopanaxadiol, an aglycosylated ginsenoside metabolite, induces hepatic stellate cell apoptosis through liver kinase B1–AMP-activated protein kinase activation

Sang Mi Park [1,☆], Eun Hye Jung [1,☆], Jae Kwang Kim [1], Kyung Hwan Jegal [1], Chung A Park [2], Il Je Cho [1,*], Sang Chan Kim [1,*]

[1] MRC-GHF, Department of Herbal Formulation, College of Korean Medicine, Daegu Haany University, Gyeongsan, Republic of Korea
[2] College of Korean Medicine, Daegu Haany University, Daegu, Republic of Korea

ARTICLE INFO

Article history:
Received 9 August 2016
Received in Revised form
7 December 2016
Accepted 19 January 2017
Available online 25 January 2017

Keywords:
AMP-activated protein kinase (AMPK)
apoptosis
hepatic stellate cells (HSCs)
liver kinase B1 (LKB1)
20S-protopanaxadiol (PPD)

ABSTRACT

Background: Previously, we reported that Korean Red Ginseng inhibited liver fibrosis in mice and reduced the expressions of fibrogenic genes in hepatic stellate cells (HSCs). The present study was undertaken to identify the major ginsenoside responsible for reducing the numbers of HSCs and the underlying mechanism involved.

Methods: Using LX-2 cells (a human immortalized HSC line) and primary activated HSCs, MTT (3-(4,5-dimethylthiazol-2-yl)-2,5-diphenyl-tetrazolium bromide) assays were conducted to examine the cytotoxic effects of ginsenosides. H_2O_2 productions, glutathione contents, lactate dehydrogenase activities, mitochondrial membrane permeabilities, apoptotic cell subpopulations, caspase-3/-7 activities, transferase dUTP nick end labeling (TUNEL) staining, and immunoblot analysis were performed to elucidate the molecular mechanism responsible for ginsenoside-mediated cytotoxicity. Involvement of the AMP-activated protein kinase (AMPK)-related signaling pathway was examined using a chemical inhibitor and small interfering RNA (siRNA) transfection.

Results and conclusion: Of the 11 ginsenosides tested, 20S-protopanaxadiol (PPD) showed the most potent cytotoxic activity in both LX-2 cells and primary activated HSCs. Oxidative stress-mediated apoptosis induced by 20S-PPD was blocked by *N*-acetyl-L-cysteine pretreatment. In addition, 20S-PPD concentration-dependently increased the phosphorylation of AMPK, and compound C prevented 20S-PPD-induced cytotoxicity and mitochondrial dysfunction. Moreover, 20S-PPD increased the phosphorylation of liver kinase B1 (LKB1), an upstream kinase of AMPK. Likewise, transfection of LX-2 cells with LKB1 siRNA reduced the cytotoxic effect of 20S-PPD. Thus, 20S-PPD appears to induce HSC apoptosis by activating LKB1–AMPK and to be a therapeutic candidate for the prevention or treatment of liver fibrosis.

1. Introduction

Liver fibrosis is the result of an excessively exuberant wound healing response to chronic hepatic damage caused by imbalance between extracellular matrix (ECM) production and degradation. ECM overproduction caused by chronic damage leads to progressive loss of hepatic parenchyma and a progressive advance to cirrhosis [1,2]. Activated hepatic stellate cells (HSCs) are one of the major executors of ECM accumulation in the liver. In their quiescent state, HSCs reside in the perisinusoidal space of Disse and store vitamin A. Repeated liver injury induces the transdifferentiation of quiescent HSCs into proliferative, contractile, and fibrogenic myofibroblast-like cells [2]. Evidence indicates that liver fibrosis is a dynamic, reversible process, and thus, reducing numbers of activated HSCs is regarded as a critical strategy for reversing liver fibrogenesis [2,3]. Although no drug has been approved for the treatment of liver fibrosis, it has been reported that several natural products, including berberine and guggulsterone, can cause the

* Corresponding authors. MRC-GHF, Department of Herbal Formulation, College of Korean Medicine, Daegu Haany University, Gyeongsan, Gyeongsangbuk-do 38610, Republic of Korea.
E-mail addresses: skek023@dhu.ac.kr (I.J. Cho), sckim@dhu.ac.kr (S.C. Kim).
☆ These authors contributed equally to this work.

http://dx.doi.org/10.1016/j.jgr.2017.01.012
p1226-8453 e2093-4947/$ – see front matter

apoptosis of activated HSCs and reduce liver fibrosis in experimental models [4,5].

AMP-activated protein kinase (AMPK), an evolutionarily conserved heterotrimeric Ser/Thr kinase, is considered a master regulator of nutritional status and energy homeostasis and is activated by several upstream kinases, including liver kinase B1 (LKB1) [6,7]. AMPK activation in liver reduces lipid synthesis by inducing the phosphorylation of acetyl-CoA carboxylase (ACC), decreases protein metabolism by inhibiting mammalian target of rapamycin complex 1 (mTORC1), induces autophagy by activating unc-51-like protein kinase 1, and protects cells and mitochondria from oxidative stress [7–9]. Thus, AMPK activation in liver relieves metabolic imbalances caused by alcohol intake or high calorie diet and protects tissues from toxic stimuli. Interestingly, activated AMPK attenuates liver fibrosis by inhibiting the proliferation of activated HSCs and ECM accumulation [10–12]. Although it has been reported that AMPK activation leads to HSC apoptosis [4,13], the relationship between AMPK activation and HSC apoptosis remains to be further established.

Ginseng, the root of *Panax ginseng* Meyer, has been used as adaptogenic agent for centuries in Korea, and modern science has shown that ginseng saponins (ginsenosides) are major active ingredients of ginseng. The ginsenosides are classified as dammarane-type, ocotillol-type, or oleanane-type oligoglycosides, and the most abundant dammarane-type ginsenosides can be further classified as protopanaxadiol (PPD) or protopanxatriol (PPT) types [14]. Although ginsenosides have been credited with the diverse pharmacological activities of ginseng [15], they are poorly absorbed in the gastrointestinal tract, and thus, the compounds responsible for the effects of orally administered ginseng are believed to be metabolites produced in the gastrointestinal tract [16–19].

Studies have shown that ginseng and ginsenosides ameliorate diverse liver diseases by inducing the activation of AMPK [20–23]. In addition, certain ginsenosides have been reported to inhibit liver fibrosis [24,25] and to induce HSC apoptosis [26]. In a previous study, we found Korean Red Ginseng inhibited liver fibrosis induced by carbon tetrachloride in mice and decreased the expressions of transforming growth factor-β (TGF-β)-dependent fibrogenic genes in HSCs [27]. Although ginseng may regress fibrosis in liver, the major ginsenosides that contribute to reductions in activated HSC numbers have yet to be identified. Thus, in the present study, we sought to identify the ginsenosides responsible for reducing the numbers of HSC and the underlying molecular mechanisms involved.

2. Materials and methods

2.1. Reagents

Korean Red Ginseng extract (RGE) was kindly provided by KT&G Central Research Institute (Daejeon, Korea), as described previously [27]. Ginsenosides (Rb1, Rb2, Rc, 20*S*-Rg3, 20*R*-Rg3, Re, Rg1) and aglycosylated metabolites [compound K (Comp. K), 20*S*-PPT, 20*R*-PPD, and 20*S*-PPD] were purchased from Ambo Institute (Daejeon, Korea) (Fig. 1). Compound C (an inhibitor of AMPK) and STO-609 (an inhibitor of Ca^{2+}/calmodulin-dependent protein kinase kinase β, CAMKKβ) were supplied by Calbiochem (San Diego, CA, USA). Anti-poly(ADP-ribose)polymerase (PARP), anti-procaspase-3, anti-phosphorylated AMPK (Thr172), anti-phosphorylated ACC (Ser79), anti-ACC, anti-phosphorylated LKB1 (Ser428), anti-LKB1, anti-Bcl-2, anti-glial fibrillary acidic protein (GFAP), and horseradish peroxidase-conjugated secondary antibodies were obtained from Cell Signaling Technology (Beverly, MA, USA). Anti-Bax and anti-AMPK antibodies were purchased from Santa Cruz Biotechnology

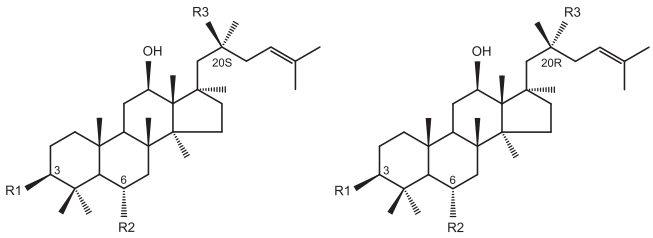

Ginsenoside	R1	R2	R3
Rb1	-O-Glc^{2}- Glc	-H	-O-Glc^{6}- Glc
Rb2	-O-Glc^{2}- Glc	-H	-O-Glc^{6}- Ara(p)
Rc	-O-Glc^{2}- Glc	-H	-O-Glc^{6}- Ara(f)
20S-Rg3	-O-Glc^{2}- Glc	-H	-H
20R-Rg3	-O-Glc^{2}- Glc	-H	-H
Comp. K	-OH	-H	-O-Glc
20S-PPD	-OH	-H	-OH
20R-PPD	-OH	-H	-OH
Re	-OH	-O-Glc^{2}- Rha	-O-Glc
Rg1	-OH	-O-Glc	-O-Glc
20S-PPT	-OH	-OH	-OH

Fig. 1. Chemical structures of ginsenosides and aglycosylated metabolites. Numerical superscripts indicate the carbons at glycosidic bonds. Ara(f), arabinofuranose; Ara(p), arabinopyranose; Comp. K, compound K; Glc, glucose; PPD, protopanaxadiol; PPT, protopanaxatriol; Rha, rhamnose.

(Santa Cruz, CA, USA). 3-(4,5-Dimethylthiazol-2-yl)-2,5-diphenyltetrazolium bromide (MTT), *N*-acetyl-L-cysteine (NAC), rhodamine123, 2′,7′-dichlorofluorescein diacetate (DCFH-DA), anti-α-smooth muscle actin (α-SMA) antibody, anti-β-actin antibody, and other reagents were purchased from Sigma-Aldrich (St. Louis, MO, USA).

2.2. Cell culture, isolation of murine primary HSCs, and treatment

LX-2 cells (a human immortalized semi-activated HSCs cell line) were kindly provided by Dr S.L. Friedman (Mount Sinai School of Medicine, New York, NY, USA). Cells were maintained in Dulbecco's modified Eagle's medium containing 10% fetal bovine serum (FBS), 2mM L-glutamine, 100 U/mL penicillin, and 100 μg/mL streptomycin at 37°C in a humidified atmosphere containing 5% CO_2. HSC isolation was conducted according to national regulations regarding the use and welfare of laboratory animals, and was approved by the Institutional Animal Care and Use Committee at Daegu Haany University (Approval No. DHU2016-061). Male ICR mice were perfused using pronase/collagenase, and primary HSCs were isolated by gradient centrifugation, as previously described [28]. Isolated cells were cultured on six-well plate in Dulbecco's modified Eagle's medium containing 10% FBS, 100 U/mL penicillin, and 100 μg/mL streptomycin for 6 d to acquire activated HSCs. The purity of isolated HSCs was confirmed by UV positivity using a fluorescent microscope (Eclipse Ti-U; Nikon, Kanagawa, Japan), and phenotypic changes during HSC activation were verified by GFAP and α-SMA immunoblotting, as previously described [13,28]. RGE and NAC were dissolved in water. Ginsenosides, DCFH-DA, rhodamine123, compound C, and STO-609 were dissolved in dimethyl sulfoxide. For all experiments, cells were grown until 80–90% confluent, incubated in medium without FBS for 12 h, and then

exposed to RGE or ginsenoside for the indicated times. Untreated cells were used as controls.

2.3. Cell viability assay

To examine the cytotoxicities of ginsenosides, cells were plated at 5×10^4 cells/well in 24-well plates, serum-starved for 12 h, and then treated with 0.3–10 mg/mL of RGE or 1–10μM of ginsenosides for the indicated times. After treatments, viable cells were stained with MTT (0.5 mg/mL, 4 h), and viabilities were assessed as previously described [8].

2.4. Preparation of whole cell lysates and immunoblot analysis

Cells were lysed in radioimmunoprecipitation buffer containing Xpert protease inhibitor cocktail (GenDEPOT, Barker, TX, USA), sodium fluoride (1mM), β-glycerophosphate (1mM), sodium orthovanadate (1mM), and sodium pyrophosphate (2.5mM). After incubation for 30 min on ice, cell lysates were collected by centrifugation at 15,000*g* for 30 min. Protein concentrations were determined using a bicinchoninic acid assay kit (Thermo, Rockford, IL, USA). Equal amounts of protein were resolved by sodium dodecyl sulfate-polyacrylamide gel electrophoresis and then transferred to nitrocellulose membranes (Amersham Biosciences, Buckinghamshire, UK). Immunoreactive proteins of interest were visualized using an enhanced chemiluminescence detection kit (Amersham Biosciences). Equal protein sample loadings in gels were verified by β-actin immunoblotting. Immunoblot intensities were quantified by densitometric analysis (Image J, rsb.info.nih.gov/ij).

2.5. Measurement of intracellular H_2O_2 production

The levels of intracellular H_2O_2 production were determined by measuring increases in dichlorofluorescein fluorescence. After treating LX-2 cells with 20*S*-PPD for 24 h, cells were stained with 20μM of DCFH-DA for 1 h. Dichlorofluorescein fluorescence was measured using an automated microplate reader (Tecan Infinite 200 PRO, Männedorf, Switzerland) at excitation/emission wavelengths of 485 nm/530 nm.

2.6. Measurement of reduced glutathione

LX-2 cells were treated with 20*S*-PPD for 24 h, and levels of reduced glutathione (GSH) were determined by using a GSH BIOXYTECH GSH-400 kit (Oxis International Inc., Portland, OR, USA). Absorbance at 405 nm was monitored using a microplate reader (Tecan).

2.7. Measurement of lactate dehydrogenase activity

Lactate dehydrogenase (LDH) activities in media were measured using an LDH assay kit (Cayman, Ann Arbor, MI, USA). Briefly, 20*S*-PPD-treated media were incubated for 30 min at room temperature with an assay buffer containing LDH diaphorase, lactic acid, NAD^+, and tetrazolium salt. Absorbance at 490 nm was then measured using a microplate reader (Tecan).

2.8. Flow cytometric analyses

Mitochondrial membrane permeability (MMP) was assessed using rhodamine123, a membrane permeable cationic fluorescent dye [8]. Cells were treated with 10μM of 20*S*-PPD for 24 h, stained with 0.05 μg/mL rhodamine123 for 1 h, and harvested by trypsinization. For some experiments, cells were pretreated either with 10mM of NAC or 3μM of compound C for 1 h, and then exposed to 10μM of 20*S*-PPD for 24 h. A dead cell apoptosis kit (Invitrogen, Carlsbad, CA, USA) was used to quantify subpopulations of apoptotic cells. Changes in MMP and dead cell subpopulations were determined using a flow cytometer (Partec, Münster, Germany). A total of 10,000 events were recorded during each analysis.

2.9. Caspase-3/-7 activities assay

Caspase-3/-7 activities in cell lysates were determined using a Caspase-Glo 3/7 assay kit (Promega, Madison, WI, USA). 20*S*-PPD-treated LX-2 cells were harvested and resuspended in phosphate-buffered saline (PBS), and Caspase-Glo 3/7 reagent was added. Cell lysates were then incubated at room temperature for 2 h, and luminescence intensities were measured using a GloMax 20/20 luminometer (Promega). Measured luminescence intensities were normalized with respect to the protein contents of lysates.

2.10. Terminal deoxynucleotidyl transferase dUTP nick end labeling staining

After treatment with 3μM or 10μM of 20*S*-PPD for 18 h, LX-2 cells were stained using an *In Situ* Apoptosis Detection Kit (Abcam, Cambridge, MA, USA). Briefly, cells were washed with PBS, fixed in PBS containing 4% paraformaldehyde, rehydrated in Tris-buffered saline, and permeabilized by adding 20 mg/mL of protease K. After inactivating endogenous peroxidase, cells were labeled with terminal deoxynucleotidyl transferase, incubated with streptoavidin–horseradish peroxidase conjugate, and then developed using diaminobenzidine. The stained cells were observed under a light microscope (Eclipse Ti-U; Nikon, Kanagawa, Japan).

2.11. Small interfering RNA transfection

Scrambled siRNA (si-Con) and small interfering RNA (siRNA) directed against LKB1 (si-LKB1) were supplied by Santa Cruz Biotechnology (Santa Cruz, CA, USA). Cells were transfected with siRNA (100 pmol each) for 24 h by using Fugene HD transfection reagent (Invitrogen), and then treated with 20*S*-PPD for the indicated times.

2.12. Statistical analysis

One-way analysis of variance was used to determine the significance level of differences between multiple group means, and unpaired Student *t* test was used to determine the significance level of differences between the means of two groups. A p value < 0.05 was considered significant.

3. Results

3.1. 20S-PPD decreased HSC viability

To explore the mechanistic basis of the antifibrotic effect of RGE, we treated LX-2 cells with 0.3–10 mg/mL of RGE, and then measured cell viability using an MTT assay. Exposure to RGE (1–10 mg/mL) for 24 h significantly and concentration-dependently decreased cell viability as compared with untreated control cells (Fig. 2A, left). When LX-2 cells were treated with 10 mg/mL of RGE for 6–48 h, cell viabilities were time-dependently decreased by RGE treatment (Fig. 2A, right). Because treatment with RGE for 24 h is sufficient incubation time to show differences in LX-2 cell viabilities, cells were treated with major ginsenosides and aglycosylated metabolites for 24 h to identify the ginsenoside responsible for RGE-mediated HSC cytotoxicity. Treatment with PPD-type

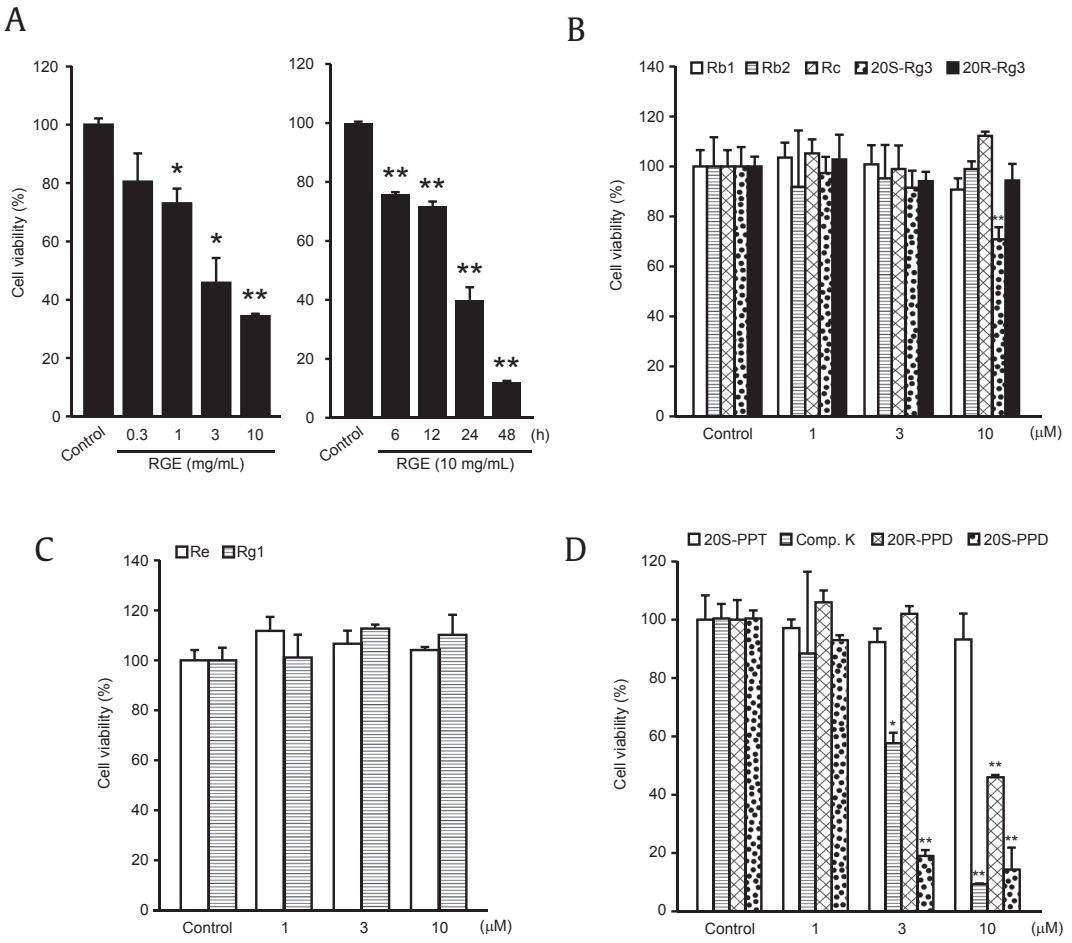

Fig. 2. Effects of Korean Red Ginseng extract (RGE) and ginsenosides on cell viability. (A) After serum starvation for 12 h, LX-2 cells were incubated with 0.3–10 mg/mL of RGE for 24 h (left) or 10 mg/mL of RGE for 6–48 h (right). (B) LX-2 cells were treated with 1–10μM of PPD-type ginsenosides for 24 h. (C) LX-2 cells were treated with 1–10μM of PPT-type ginsenosides for 24 h. (D) LX-2 cells were treated with 1–10μM of aglycosylated metabolites. Cell viabilities were measured using an MTT assay. Data represent the means ± SDs of three separate experiments. Significant versus untreated controls; * $p < 0.05$, ** $p < 0.01$. MTT, 3-(4,5-dimethylthiazol-2-yl)-2,5-diphenyl-tetrazolium bromide; SD, standard deviation; PPD, protopanaxadiol; PPT, protopanaxatriol.

ginsenosides (Rb1, Rb2, Rc, and 20*R*-Rg3) or PPT-type ginsenosides (Re and Rg1) at concentrations up to 10μM for 24 h did not affect LX-2 cell viability (Figs. 2B and 2C). However, treatment with the PPD-type ginsenoside 20*S*-Rg3 (10μM) significantly decreased cell viability. In addition, treatments with aglycosylated metabolites (Comp. K, 20*R*-PPD, and 20*S*-PPD) for 24 h also concentration-dependently reduced LX-2 cell viability, whereas treatment with 20*S*-PPT did not (Fig. 2D). The IC_{50} values of Comp. K, 20*R*-PPD, and 20*S*-PPD were 3.39 ± 0.87μM, 8.52 ± 0.59μM, and 2.05 ± 0.59μM, respectively.

Ginsenoside Rb1 has an O-linked di-glucose residue at C3 and C20 on its PPD scaffold. By contrast, the ginsenoside metabolite Comp. K has a hydroxyl group at C3 and an O-linked glucose at C20, and 20*S*-PPD has only hydrogen at C3 and C20 (Fig. 1). To examine the effect of ginsenoside aglycosylation on LX-2 cell viability, we treated cells with Rb1, Comp. K, or 20*S*-PPD (3μM each). As was expected, treatment time with Rb1 (3μM) for up to 24 h did not decrease cell viability. When LX-2 cells were incubated with 3μM of 20*S*-PPD, cell viability was reduced significantly at 6 h, and this then gradually decreased. However, cell viability started to decrease significantly at 12 h after LX-2 cells were treated with 3μM of Comp. K (Fig. 3A). The viabilities of 20*S*-PPD- and Comp. K-treated cells at 24 h were 14.75 ± 1.00% and 55.40 ± 5.17% of that of controls, respectively. Next, we isolated primary HSCs from ICR mice and cultivated them for 6 d to activate the cells. Cell purity and identity were confirmed by UV positivity, GFAP (a marker of quiescent HSCs), and α-SMA (a marker of activated HSCs) immunoblotting (Fig. 3B, upper). When primary activated HSCs were treated with Rb1, Comp. K, or 20*S*-PPD (3μM each) for 24 h, 20*S*-PPD was found to reduce α-SMA protein levels (Fig. 3B, lower). In addition, 20*S*-PPD (3μM, 24 h) had the most potent cytotoxic effect against primary activated HSCs (Fig. 3C).

3.2. 20S-PPD promoted oxidative stress

To determine whether oxidative stress was involved in 20*S*-PPD-mediated HSC death, LX-2 cells were pretreated with NAC (10mM; a representative antioxidant) and then incubated with 10μM of 20*S*-PPD for 24 h. We found that 20*S*-PPD-mediated cytotoxicity was significantly inhibited by NAC pretreatment (Fig. 4A). Next, we monitored intracellular H_2O_2 production using DCFH-DA. Treatment with 1–10μM of 20*S*-PPD for 24 h increased intracellular H_2O_2 production in a concentration-dependent manner. However, NAC pretreatment completely abolished the H_2O_2 accumulation induced by 20*S*-PPD (Fig. 4B). We also measured the level of reduced GSH (a major endogenous antioxidant that regulates redox homeostasis by scavenging reactive oxygen species). Intracellular concentrations of reduced GSH were

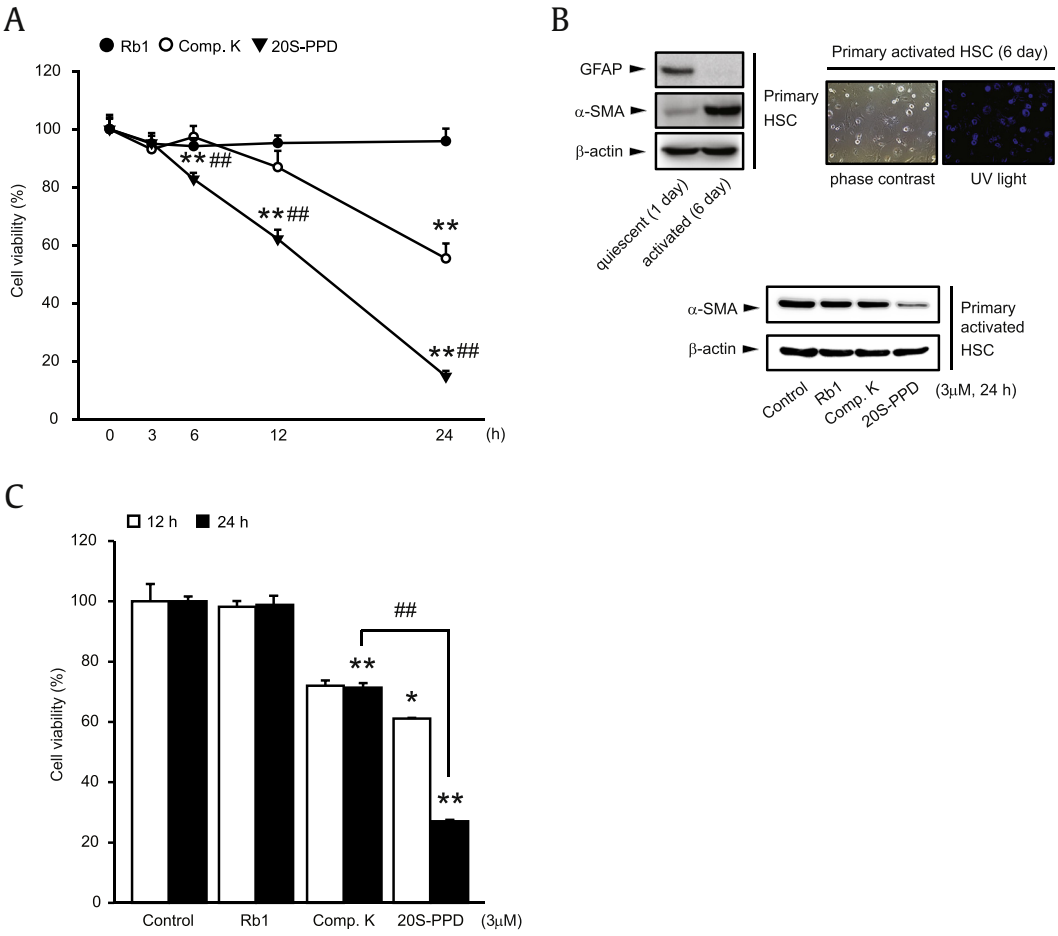

Fig. 3. Effects of aglycosylated metabolites on HSC viability. (A) LX-2 cells were treated with Rb1, Comp. K, or 20*S*-PPD (3μM each) for the indicated times, and then cell viabilities were measured. (B) Primary HSCs were isolated from ICR mice and continuously cultivated for 6 d to acquire activated HSCs. Purity and phenotypic changes of activated HSCs were confirmed by UV positivity, and by immunoblotting for GFAP and α-SMA (upper). Primary activated HSCs were treated with 3μM of Rb1, Comp. K, or 20*S*-PPD for 24 h, α-SMA protein levels were assessed by immunoblotting. Equal protein loadings were verified by immunoblotting for β-actin (lower). (C) Effect of Rb1, Comp. K, or 20*S*-PPD on the cell viabilities of primary activated HSCs. Data represent the means ± SDs of three separate experiments. Significant versus untreated controls; * $p < 0.05$, ** $p < 0.01$; significant as compared between Comp. K- and 20*S*-PPD-treated cells, $^{\#\#}$ $p < 0.01$. Comp. K, compound K; GFAP, glial fibrillary acidic protein; HSC, hepatic stellate cell; PPD, protopanaxadiol; SMA, smooth muscle actin; SD, standard deviation.

significantly diminished after treatment of LX-2 cells with 3μM or 10μM of 20*S*-PPD for 24 h (Fig. 4C). In addition, we further investigated whether reactive oxygen species generation by 20*S*-PPD was mediated by mitochondrial membrane dysfunction. We observed that 20*S*-PPD (10μM) significantly increased LX-2 cell populations with low rhodamine123 fluorescence intensity as compared with controls, and that this 20*S*-PPD-induced change was prevented by NAC pretreatment (10mM) (Fig. 4D). Furthermore, LX-2 cells treated with 20*S*-PPD released LDH to medium in a concentration-dependent manner (Fig. 4E).

3.3. 20*S*-PPD induced HSC apoptosis

To determine the type of cell death induced by 20*S*-PPD, LX-2 cells were treated with 3μM or 10μM of 20*S*-PPD for 24 h and double stained with fluorescein isothiocyanate-conjugated annexin V and propidium iodide (PI). Cell subpopulations were then investigated by flow cytometry (Fig. 5A). The results showed that 20*S*-PPD concentration-dependently increased the proportion of early apoptotic cells (annexin V-positive and PI-negative stained cells). Proportions of early apoptosis were 25.12 ± 12.47% and 63.03 ± 12.70% in cells treated with 3μM or 10μM of 20*S*-PPD, respectively. Next, we monitored the expression levels of apoptosis-related proteins to confirm apoptosis induction by 20*S*-PPD. When cells were treated with Comp. K or 20*S*-PPD (both at 3μM) for 24 h, 20*S*-PPD was found to cause more PARP cleavage than Comp. K. Although Comp. K treatment tended to increase PARP cleavage as compared with controls, no statistical difference was observed (Fig. 5B). Furthermore, 20*S*-PPD increased Bax expression, reduced the expressions of procaspase-3 and Bcl-2 in a concentration-dependent manner (Fig. 5C), and significantly increased caspase-3/-7 activities (Fig. 5D) and transferase dUTP nick end labeling (TUNEL) staining intensities of LX-2 cells (Fig. 5E).

3.4. AMPK activation was involved in 20*S*-PPD-mediated apoptosis

To determine whether 20*S*-PPD activates AMPK in HSCs, we monitored the phosphorylations of AMPK and ACC (a downstream substrate of AMPK) in LX-2 cells. The phosphorylations of AMPK and ACC were both increased by 20*S*-PPD at concentrations of 1–10μM, whereas 20*S*-PPD did not affect the expression levels of AMPK and ACC (Fig. 6A, upper). Maximum AMPK phosphorylation was observed after treatment with 1μM of 20*S*-PPD for 6 h, and this phosphorylation was sustained for 24 h (Fig. 6A, lower). Consistently, treatment with 20*S*-PPD increased the phosphorylations of AMPK and ACC more than the same concentrations of Rb1 or Comp.

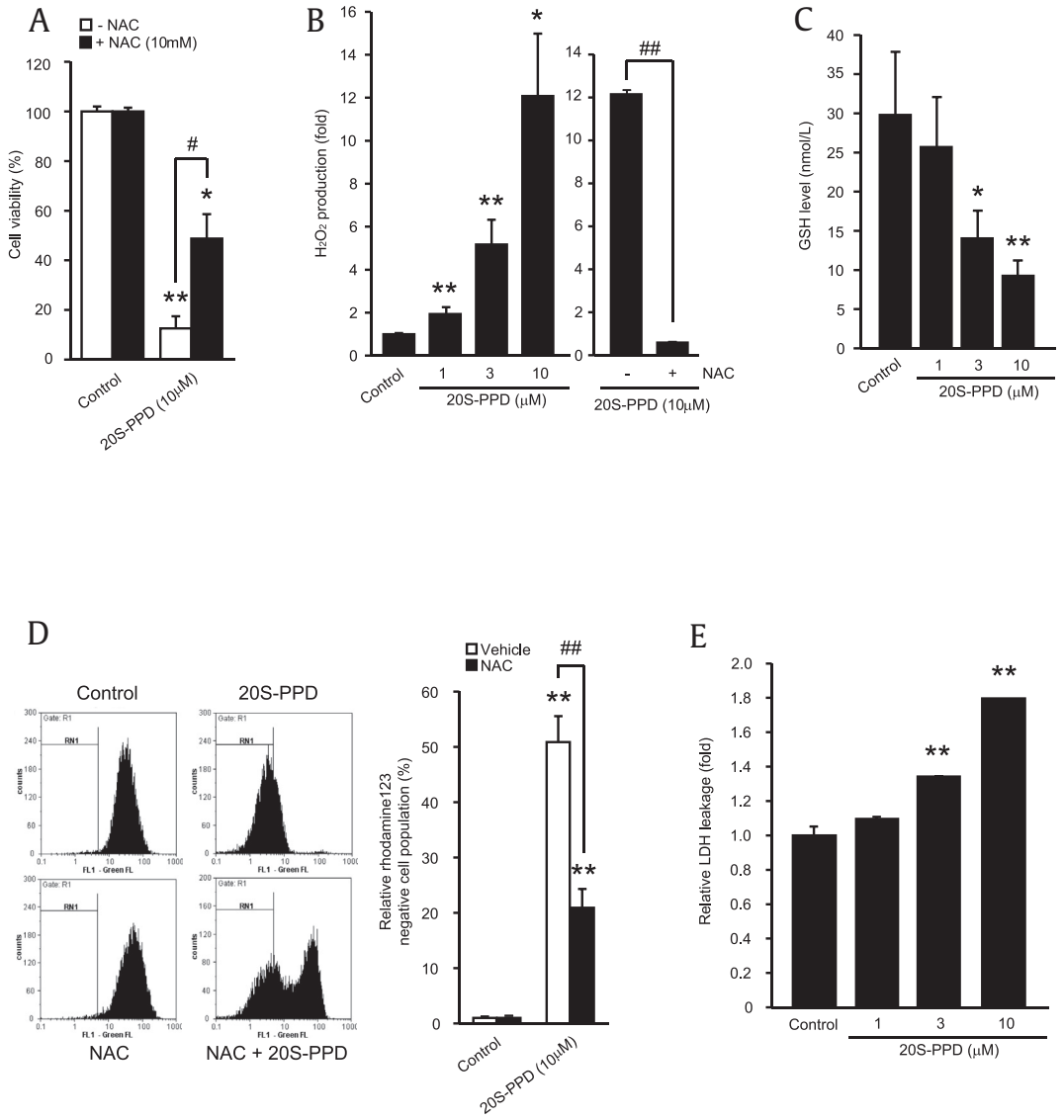

Fig. 4. Induction of oxidative stress by 20*S*-PPD. (A) Effect of NAC on 20*S*-PPD-mediated cytotoxicity. LX-2 cells were pretreated with 10mM of NAC for 1 h and then further incubated with 10μM of 20*S*-PPD for 24 h. (B) H_2O_2 production by 20*S*-PPD. (C) GSH contents of cells treated with 1–10μM of 20*S*-PPD for 24 h. (D) MMPs. Treated cells were stained with rhodamine123 (0.05 μg/mL) and then MMPs were assessed (left). Cell populations that exhibited low rhodamine123 intensity were quantified by flow cytometry (right). (E) LDH leakage. Conditioned media of cells treated with 1–10μM of 20*S*-PPD were collected, and LDH activities were measured. Data represent the means ± SDs of three separate experiments. Significant versus untreated controls or treatment with NAC alone, * $p < 0.05$, ** $p < 0.01$; significant as compared between 20*S*-PPD alone and 20*S*-PPD plus NAC treated cells, $^{\#}$ $p < 0.05$, $^{\#\#}p < 0.01$. GSH, glutathione; LDH, lactate dehydrogenase; MMP, mitochondrial membrane permeability; NAC, *N*-acetyl-L-cysteine; PPD, protopanaxadiol; SD, standard deviation.

K in LX-2 cells and primary activated HSCs (Fig. 6B). To investigate the role of AMPK activation in 20*S*-PPD-induced HSCs apoptosis, AMPK activation was blocked by pretreating LX-2 cells with compound C, and 20*S*-PPD-mediated cytotoxicity was then monitored. Cell viability results showed that pretreatment with compound C (1μM or 3μM) significantly inhibited the 20*S*-PPD-induced apoptosis of LX-2 cells (Fig. 6C, lower). Inhibition of AMPK activity by compound C was confirmed by immunoblotting (Fig. 6C, upper). Treatment with compound C alone did not alter cell viability (data not shown). Furthermore, mitochondrial impairment induced by 20*S*-PPD was also significantly attenuated by compound C pretreatment (Fig. 6D).

3.5. 20S-PPD phosphorylated AMPK by activating LKB1

To identify the upstream kinase involved in 20*S*-PPD-mediated AMPK activation, we investigated whether LKB1 (an upstream kinase of AMPK) was phosphorylated by 20*S*-PPD. LKB1 phosphorylation started to increase at 6 h after treating LX-2 cells with 1μM of 20*S*-PPD and was sustained for up to 24 h (Fig. 7A), which paralleled 20*S*-PPD-induced AMPK phosphorylation (Fig. 6A). Transfection with LKB1 siRNA decreased 20*S*-PPD-mediated AMPK phosphorylation (Fig. 7B), and inhibited 20*S*-PPD-mediated cytotoxicity (Fig. 7C). However, chemical inhibition of CAMKKβ by STO-609 had no effect on 20*S*-PPD-mediated AMPK phosphorylation or cytotoxicity (Fig. 7D).

4. Discussion

It is generally accepted that the diverse pharmacological activities of *P. ginseng* are derived from a group of steroidal saponins, the ginsenosides [15]. When *P. ginseng* is orally administered, ginsenosides cannot be easily absorbed into tissues because of their hydrophilicities. Thus, ginsenosides are converted into metabolites

in the gastrointestinal tract by acid hydrolysis or intestinal microflora. It has been reported that the fully aglycosylated metabolite, PPD, can be produced from ginseng extract, Rb1, Rg3, or Comp. K by intestinal microflora [16,18,19,29], and that aglycosylated metabolites are more potent than their parent compounds [26,29,30]. Studies have shown that 20*S*-PPD inhibits the growth of *Helicobacter pylori* [29], attenuates the progression and growth of castration-resistant prostate cancer [31], enhances the sensitivity of chemotherapy against colorectal cancer [16], and protects neurons from permanent focal cerebral ischemic damage [32]. Although Park et al [26] reported that Comp. K triggers apoptosis in T-HSC/Cl-6 cells (a rat-derived HSC line), the effects of other ginsenosides on HSCs remain to be established.

Among the 11 ginsenosides and aglycosylated metabolites tested, we found that 20*S*-PPD exhibited the greatest cytotoxic activity in HSCs (Figs. 2, 3). Our results indicate that 20*S*-PPD increased H_2O_2 production, depleted GSH levels, impaired MMP, and enhanced LDH leakage. Furthermore, pretreatment with NAC attenuated 20*S*-PPD-mediated H_2O_2 production, mitochondrial dysfunction, and cytotoxicity (Fig. 4), indicating that oxidative stress is involved in HSC death. Oxidative stress changes the Bcl-2/Bax expression ratio and opens the mitochondrial permeability

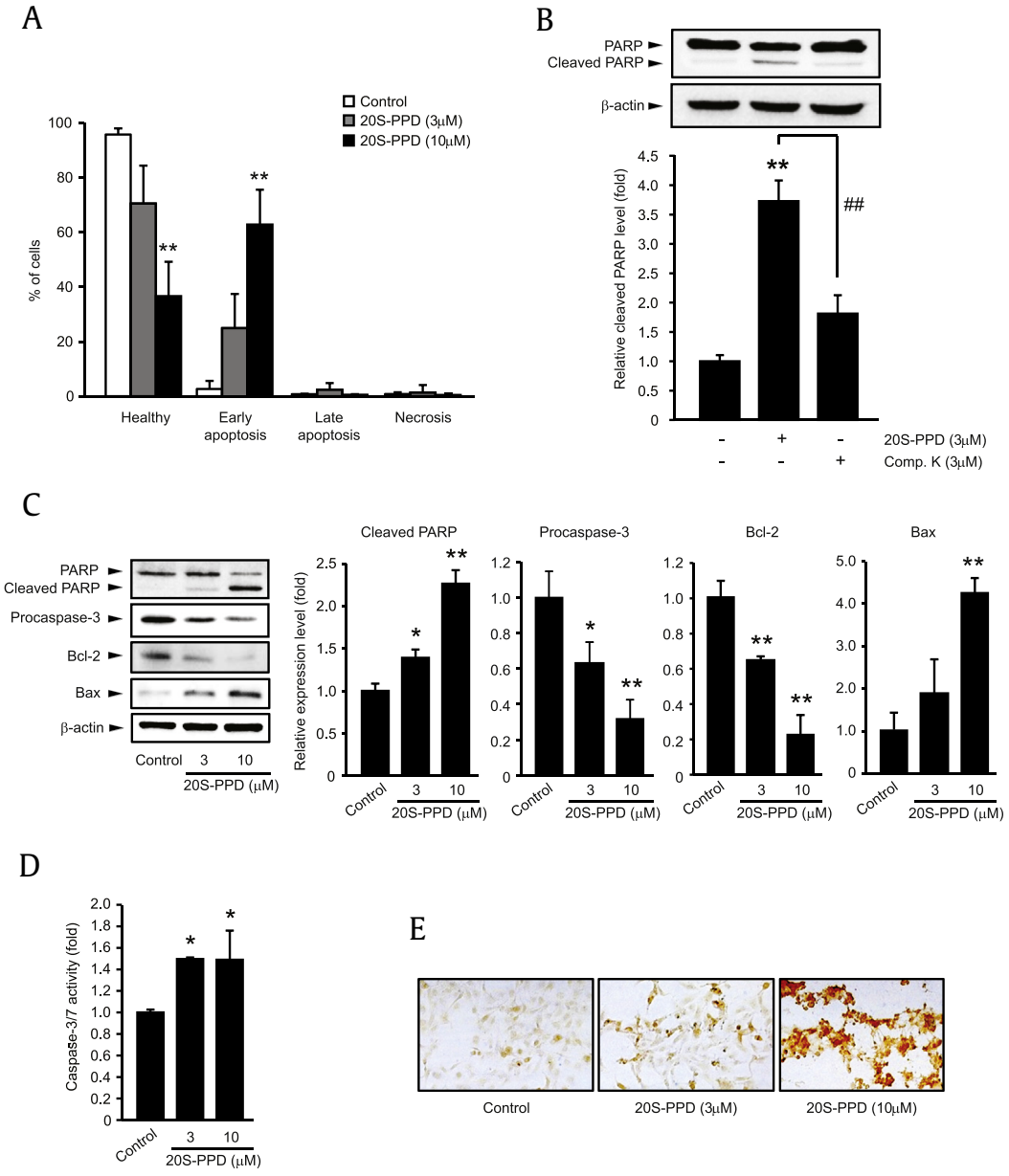

Fig. 5. Induction of apoptosis by 20*S*-PPD. (A) Flow cytometry analyses of cells double stained with fluorescein isothiocyanate-conjugated annexin V and PI. LX-2 cells were treated with 3μM or 10μM of 20*S*-PPD for 24 h. Percentages of healthy (low annexin V and low PI stained cells), early apoptotic (high annexin V and low PI stained cells), late apoptotic (high annexin V and high PI stained cells), and necrotic (low annexin V and high PI stained cells) cells were shown in the bar graph. (B) PARP cleavage. LX-2 cells were treated with 20*S*-PPD or Comp. K (3μM each) for 24 h and cell lysates were immunoblotted for PARP. (C) Expressions of apoptosis-related proteins. LX-2 cells were treated with 3μM or 10μM 20*S*-PPD for 24 h and immunoblotted for proteins associated with apoptosis. (D) Caspase-3/-7 activities. (E) TUNEL staining. LX-2 cells were treated with 3μM or 10μM 20*S*-PPD for 18 h and then stained by TUNEL. The relative expression levels of proteins were determined by scanning densitometry (B and C). Data represent the means ± SDs of three separate experiments. Significant versus untreated controls, * $p < 0.05$, ** $p < 0.01$; significant as compared between 20*S*-PPD and Comp. K treated cells, ## $p < 0.01$. Comp. K, compound K; PARP, poly(ADP-ribose)polymerase; PI, propidium iodide; PPD, protopanaxadiol; SD, standard deviation; TUNEL, transferase dUTP nick end labeling.

transition pore, which promotes caspase-dependent apoptosis [33,34]. Caspase-3 and caspase-7 are executor caspases and are responsible for the cleavage of more than 100 different proteins including that of PARP [35]. PARP cleavage causes defects in the DNA repair system and accelerates DNA fragmentation [36]. In accord with previous reports, the present study shows that 20S-PPD concentration-dependently reduced the expression of Bcl-2 (an antiapoptotic protein), increased the expression of Bax (a pro-apoptotic protein), and enhanced caspase-3/-7 activities. In addition, 20S-PPD concentration-dependently increased PARP cleavage, TUNEL staining intensity, and the proportions of early apoptotic cells (Fig. 5). Moreover, 20S-PPD induced the cleavage of PARP more than Comp. K at same concentration (Fig. 5B), which suggests that the apoptotic activities of ginsenosides are potentiated by the loss of sugar moieties.

Accumulated evidence shows AMPK is a double-edged sword in terms of determining the fate of cells against a variety of stresses. Previously, we reported that AMPK activation by several natural products protects hepatocytes from oxidative stress [8,37]. In addition, other groups have reported that AMPK activation attenuates hepatocytes apoptosis in different experimental models, such as tumor necrosis factor α-induced hepatitis and hepatic ischemia–reperfusion [38,39]. However, AMPK activation in hepatocellular carcinoma cells causes cell cycle arrest and apoptosis [40,41]. AMPK

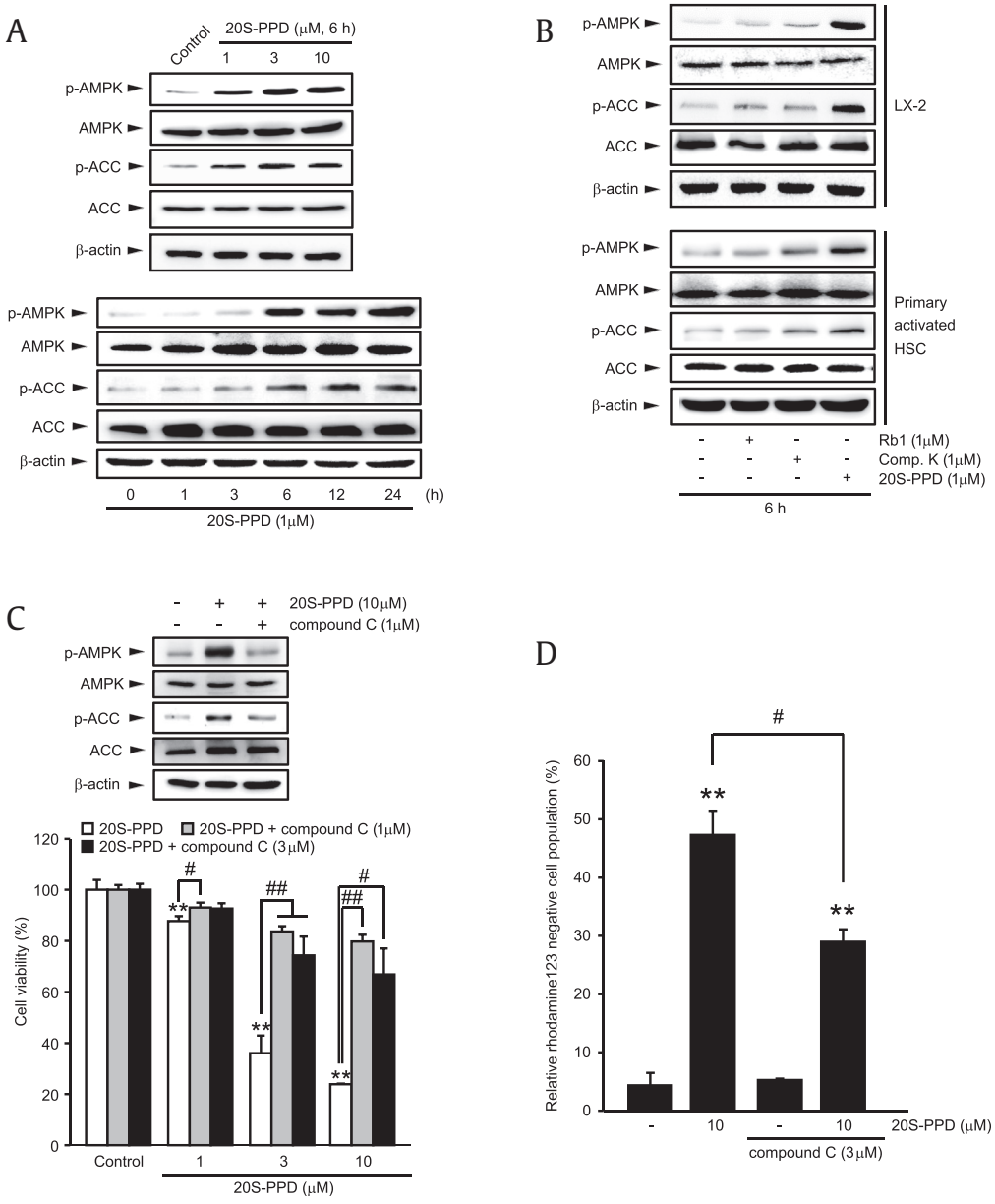

Fig. 6. Activation of AMPK by 20S-PPD. (A) AMPK activation. LX-2 cells were treated with 1–10μM of 20S-PPD for 6 h (upper) or 1μM of 20S-PPD for 1–24 h (lower). Levels of phosphorylated AMPK and ACC in cell lysates were assessed by immunoblotting. Equal protein loadings was confirmed by immunoblotting for β-actin. Results were confirmed by repeated experiments. (B) Effect of aglycosylated ginsenosides on AMPK activation. LX-2 cells (upper) or primary activated HSCs (lower) were treated with Rb1, Comp. K or 20S-PPD (1μM each) for 6 h. (C) The effects of compound C on 20S-PPD-mediated cytotoxicity. LX-2 cells were pretreated with 1μM or 3μM of compound C for 1 h, and subsequently exposed to 1–10μM of 20S-PPD for 24 h. (D) Effect of compound C on 20S-PPD-mediated mitochondrial dysfunction. LX-2 cells were pretreated with 3μM of compound C for 1 h and then incubated with 10μM of 20S-PPD for 24 h. Data represent the means ± SDs of three separate experiments. Significant versus untreated controls or treatment with compound C alone, $^{**}p < 0.01$; significant as compared between 20S-PPD alone and 20S-PPD plus compound C treated cells, $^{\#}p < 0.05$, $^{\#\#}p < 0.01$. ACC, acetyl-CoA carboxylase; AMPK, AMP-activated protein kinase; Comp. K, compound K; HSCs, hepatic stellate cells; PPD, protopanaxadiol; SD, standard deviation.

suppresses proliferation, migration, chemokine secretion, and profibrogenic genes expressions in HSCs [10–12,42,43], which are the major phenotype changes observed during HSC activation [3]. Blockage of AMPK has been reported to attenuate the ability of adiponectin to inhibit HSC proliferation [11,12], and AMPK activation in HSCs degrades p300 coactivator, dissociates protein interactions between Smad3 and p300, and thereby inhibits the TGF-β-mediated expressions of ECM proteins [10]. Furthermore, AMPK activation by curcumin in HSCs upregulates antioxidant and adipogenic genes by inducing peroxisome proliferator-activated receptor-γ coactivator-1α, and downregulates the expressions of profibrogenic genes by inhibiting aerobic glycolysis [42,43].

Although several studies have suggested that AMPK activation leads to HSC apoptosis [4,13], the relationship between AMPK activation and HSC apoptosis remains to be further established. The present results indicate that 20*S*-PPD was the most cytotoxic and that it also triggered AMPK phosphorylation in HSCs (Figs. 3, 6B). Moreover, 20*S*-PPD-mediated mitochondrial dysfunction and apoptosis were blocked in the presence of compound C (an AMPK inhibitor) (Figs. 6C and 6D). Therefore, our results imply that AMPK activation is involved in the 20*S*-PPD-mediated apoptosis of HSCs. mTORC1 is another regulator of cell growth in response to energy status or environmental stress [44]. mTORC1 is a protein complex that contains mTOR, regulatory associated protein of mTOR (raptor), GβL, and PRAS40 [44,45]. AMPK activation inhibits mTORC1 activity and that of its downstream kinase, p70 ribosomal S6 kinase, via the phosphorylation of raptor [46]. Our supplementary results indicate that 20*S*-PPD increased the phosphorylation of raptor, decreased the GβL expression, and reduced levels of phosphorylated mTOR and S6 (a downstream substrate of p70 ribosomal S6 kinase) in LX-2 cells (Fig. S1). Although identities of the downstream signaling molecules that regulate HSC apoptosis

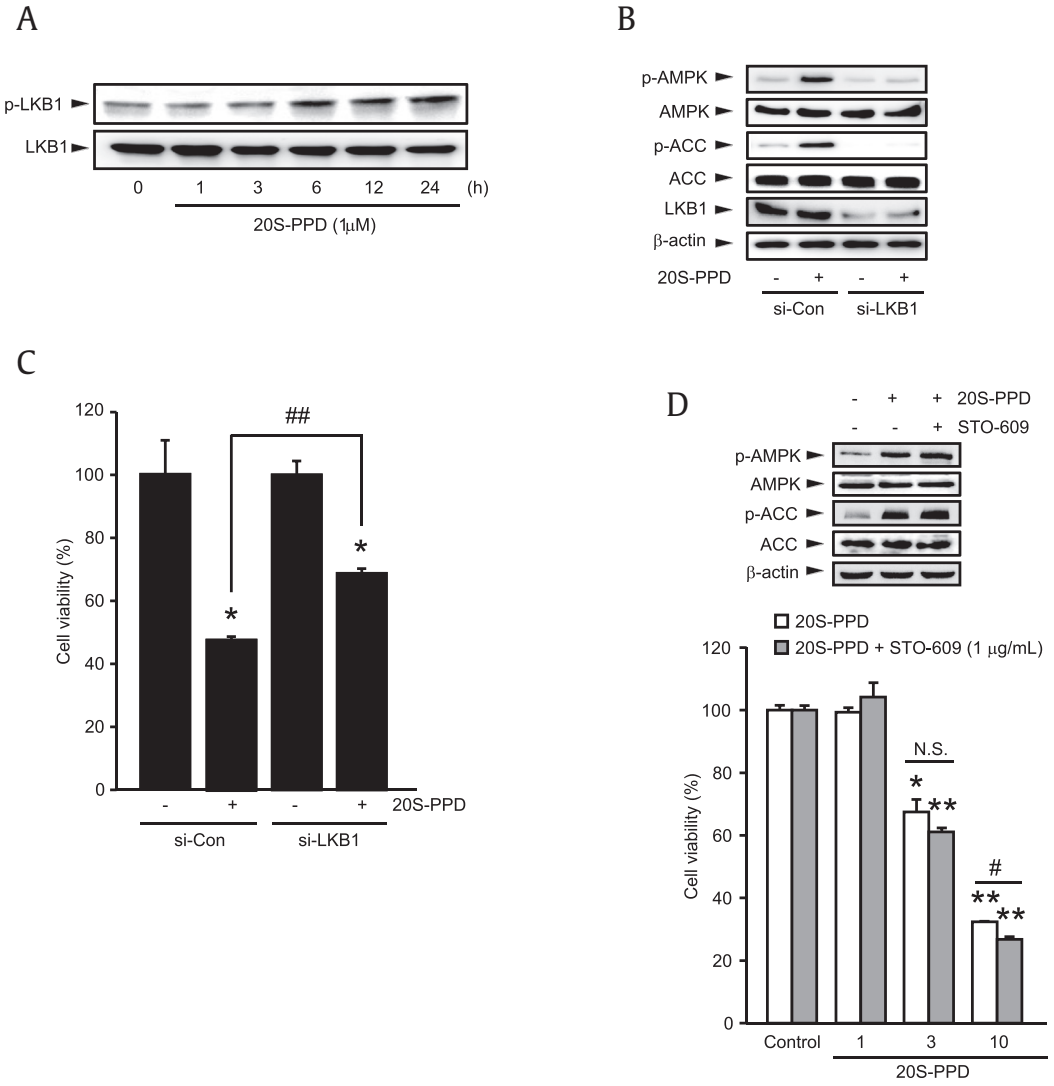

Fig. 7. Role of LKB1 on 20*S*-PPD-mediated AMPK activation. (A) LKB1 phosphorylation. LX-2 cells were treated with 20*S*-PPD (1μM) for the indicated times. Levels of phosphorylated LKB1 in cell lysates were measured by immunoblotting. Equal protein loadings were confirmed by immunoblotting for LKB1. (B) Effect of LKB1 knockdown on 20*S*-PPD-mediated AMPK activation. LX-2 cells were transfected with scrambled siRNA (si-Con) or LKB1 siRNA (si-LKB1) and then treated with 20*S*-PPD (10μM) for 6 h. (C) Effect of LKB1 knockdown on 20*S*-PPD-mediated cytotoxicity. si-LKB1 transfected cells were treated with 10μM of 20*S*-PPD for 24 h and cell viabilities were measured. (D) Effect of STO-609 on 20*S*-PPD-mediated cytotoxicity. LX-2 cells were pretreated with 1 μg/mL STO-609 and then exposed to 10μM of 20*S*-PPD for 6 h (upper) or to 1–10μM of 20*S*-PPD for 24 h (lower). Data represent the means ± SDs of three separate experiments. Significant versus untreated controls, $^{*}p < 0.05$, $^{**}p < 0.01$; significant as compared between 20*S*-PPD-treated cells, $^{\#}p < 0.05$, $^{\#\#}p < 0.01$. ACC, acetyl-CoA carboxylase; AMPK, AMP-activated protein kinase; LKB1, liver kinase B1; PPD, protopanaxadiol; N.S., not significant; SD, standard deviation.

remain to be further identified, our findings suggest the involvement of mTORC1 inhibition in AMPK-mediated apoptosis induced by 20*S*-PPD.

Changes in AMP/ATP ratio and the activations of LKB1, CaMKK, protein kinase A, and TGF-β-activated kinase have been reported to regulate AMPK activity [6,7,47]. Ginsenosides and aglycosylated metabolites activate AMPK via multiple upstream activators [22]. It has been established that LKB1 activation by Rg1 or Rg2 inhibits hepatic glucose production [23,48]. Comp. K decreases matrix methaloprotease-1 expression in fibroblasts by activating LKB1 [30]. However, the activations of CaMKK by Comp. K or Rg3 induce the apoptosis of colon cancer cells and increase nitric oxide production in endothelial cells, respectively [49,50]. In the present study, 20*S*-PPD increased LKB1 phosphorylation and concomitantly increased AMPK phosphorylation. In addition, AMPK phosphorylation and HSC apoptosis by 20*S*-PPD were attenuated in si-LKB1 transfected cells. However, the chemical inhibition of CaMKKβ by STO-609 did not decrease 20*S*-PPD-mediated AMPK phosphorylation or cytotoxicity in LX-2 cells (Fig. 7). Therefore, our results suggest that 20*S*-PPD activates AMPK in HSCs in an LKB1-dependent manner.

In conclusion, our results demonstrate that aglycosylation potentiates the cytotoxicities of ginsenosides against HSCs. Of the ginsenosides examined in the present study, 20*S*-PPD most potently induced the apoptosis of HSCs via LKB1-dependent AMPK activation. Taken together, these findings suggest that 20*S*-PPD is a potential therapeutic candidate for the prevention or treatment of liver fibrosis.

Conflicts of interests

The authors declare that they have no conflicts of interests.

Acknowledgments

This study was supported by the National Research Foundation (NRF) of Korea funded by Korea government (MSIP) (Grant No. 2012 R1A5A2A42671316) and partly by a grant from Daegu Haany University Kylin Foundation in 2014.

Appendix A. Supplementary data

Supplementary data related to this article can be found at http://dx.doi.org/10.1016/j.jgr.2017.01.012.

References

[1] Moreira RK. Hepatic stellate cells and liver fibrosis. Arch Pathol Lab Med 2007;131:1728–34.
[2] Bataller R, Brenner DA. Liver fibrosis. J Clin Invest 2005;115:209–18.
[3] Lee YA, Wallace MC, Friedman SL. Pathobiology of liver fibrosis: a translational success story. Gut 2015;64:830–41.
[4] Wang N, Xu Q, Tan HY, Hong M, Li S, Yuen MF, Feng Y. Berberine inhibition of fibrogenesis in a rat model of liver fibrosis and in hepatic stellate cells. Evid Based Complement Alternat Med 2016;2016:8762345.
[5] Kim BH, Yoon JH, Yang JI, Myung SJ, Lee JH, Jung EU, Yu SJ, Kim YJ, Lee HS, Kim CY. Guggulsterone attenuates activation and survival of hepatic stellate cell by inhibiting nuclear factor kappa B activation and inducing apoptosis. J Gastroenterol Hepatol 2013;28:1859–68.
[6] Lage R, Diéguez C, Vidal-Puig A, López M. AMPK: a metabolic gauge regulating whole-body energy homeostasis. Trends Mol Med 2008;14:539–49.
[7] Kahn BB, Alquier T, Carling D, Hardie DG. AMP-activated protein kinase: ancient energy gauge provides clues to modern understanding of metabolism. Cell Metab 2005;1:15–25.
[8] Ko HL, Jung EH, Jung DH, Kim JK, Ku SK, Kim YW, Kim SC, Zhao R, Lee CW, Cho IJ. *Paeonia japonica* root extract protects hepatocytes against oxidative stress through inhibition of AMPK-mediated GSK3β. J Funct Foods 2016;20:303–16.
[9] Egan D, Kim J, Shaw RJ, Guan KL. The autophagy initiating kinase ULK1 is regulated via opposing phosphorylation by AMPK and mTOR. Autophagy 2011;7:643–4.
[10] Lim JY, Oh MA, Kim WH, Sohn HY, Park SI. AMP-activated protein kinase inhibits TGF-β-induced fibrogenic responses of hepatic stellate cells by targeting transcriptional coactivator p300. J Cell Physiol 2012;227:1081–9.
[11] Adachi M, Brenner DA. High molecular weight adiponectin inhibits proliferation of hepatic stellate cells via activation of adenosine monophosphate-activated protein kinase. Hepatology 2008;47:677–85.
[12] Caligiuri A, Bertolani C, Guerra CT, Aleffi S, Galastri S, Trappoliere M, Vizzutti F, Gelmini S, Laffi G, Pinzani M, et al. Adenosine monophosphate-activated protein kinase modulates the activated phenotype of hepatic stellate cells. Hepatology 2008;47:668–76.
[13] Ding X, Saxena NK, Lin S, Xu A, Srinivasan S, Anania FA. The roles of leptin and adiponectin: a novel paradigm in adipocytokine regulation of liver fibrosis and stellate cell biology. Am J Pathol 2005;166:1655–69.
[14] Kim DH. Chemical diversity of *Panax ginseng, Panax quinquifolium*, and *Panax notoginseng*. J Ginseng Res 2012;36:1–15.
[15] Attele AS, Wu JA, Yuan CS. Ginseng pharmacology: multiple constituents and multiple actions. Biochem Pharmacol 1999;58:1685–93.
[16] Wang CZ, Zhang Z, Wan JY, Zhang CF, Anderson S, He X, Yu C, He TC, Qi LW, Yuan CS. Protopanaxadiol, an active ginseng metabolite, significantly enhances the effects of fluorouracil on colon cancer. Nutrients 2015;7:799–814.
[17] Wan JY, Liu P, Wang HY, Qi LW, Wang CZ, Li P, Yuan CS. Biotransformation and metabolic profile of American ginseng saponins with human intestinal microflora by liquid chromatography quadrupole time-of-flight mass spectrometry. J Chromatogr A 2013;1286:83–92.
[18] Bae EA, Park SY, Kim DH. Constitutive beta-glucosidases hydrolyzing ginsenoside Rb1 and Rb2 from human intestinal bacteria. Biol Pharm Bull 2000;23:1481–5.
[19] Hasegawa H, Sung JH, Matsumiya S, Uchiyama M. Main ginseng saponin metabolites formed by intestinal bacteria. Planta Med 1996;62:453–7.
[20] Xin Y, Wei J, Chunhua M, Danhong Y, Jianguo Z, Zongqi C, Jian-An B. Protective effects of ginsenoside Rg1 against carbon tetrachloride-induced liver injury in mice through suppression of inflammation. Phytomedicine 2016;23:583–8.
[21] Han JY, Lee S, Yang JH, Kim S, Sim J, Kim MG, Jeong TC, Ku SK, Cho IJ, Ki SH. Korean Red Ginseng attenuates ethanol-induced steatosis and oxidative stress via AMPK/Sirt1 activation. J Ginseng Res 2015;39:105–15.
[22] Jeong KJ, Kim GW, Chung SH. AMP-activated protein kinase: an emerging target for ginseng. J Ginseng Res 2014;38:83–8.
[23] Yuan HD, Kim DY, Quan HY, Kim SJ, Jung MS, Chung SH. Ginsenoside Rg2 induces orphan nuclear receptor SHP gene expression and inactivates GSK3β via AMP-activated protein kinase to inhibit hepatic glucose production in HepG2 cells. Chem Biol Interact 2012;195:35–42.
[24] Hou YL, Tsai YH, Lin YH, Chao JC. Ginseng extract and ginsenoside Rb1 attenuate carbon tetrachloride-induced liver fibrosis in rats. BMC Complement Altern Med 2014;14:415.
[25] Geng J, Peng W, Huang Y, Fan H, Li S. Ginsenoside-Rg1 from *Panax notoginseng* prevents hepatic fibrosis induced by thioacetamide in rats. Eur J Pharmacol 2010;634:162–9.
[26] Park EJ, Zhao YZ, Kim J, Sohn DH. A ginsenoside metabolite, 20-*O*-beta-d-glucopyranosyl-20(*S*)-protopanaxadiol, triggers apoptosis in activated rat hepatic stellate cells via caspase-3 activation. Planta Med 2006;72:1250–3.
[27] Ki SH, Yang JH, Ku SK, Kim SC, Kim YW, Cho IJ. Red ginseng extract protects against carbon tetrachloride-induced liver fibrosis. J Ginseng Res 2013;37:45–53.
[28] Cho IJ, Kim YW, Han CY, Kim EH, Anderson RA, Lee YS, Lee CH, Hwang SJ, Kim SG. E-cadherin antagonizes transforming growth factor β1 gene induction in hepatic stellate cells by inhibiting RhoA-dependent Smad3 phosphorylation. Hepatology 2010;52:2053–64.
[29] Bae EA, Han MJ, Choo MK, Park SY, Kim DH. Metabolism of 20(*S*)- and 20(*R*)-ginsenoside Rg3 by human intestinal bacteria and its relation to in vitro biological activities. Biol Pharm Bull 2002;25:58–63.
[30] Shin DJ, Kim JE, Lim TG, Jeong EH, Park G, Kang NJ, Park JS, Yeom MH, Oh DK, Bode AM, et al. 20-*O*-β-d-Glucopyranosyl-20(*S*)-protopanaxadiol suppresses UV-Induced MMP-1 expression through AMPK-mediated mTOR inhibition as a downstream of the PKA-LKB1 pathway. J Cell Biochem 2014;115:1702–11.
[31] Cao B, Qi Y, Yang Y, Liu X, Xu D, Guo W, Zhan Y, Xiong Z, Zhang A, Wang AR, et al. 20(*S*)-Protopanaxadiol inhibition of progression and growth of castration-resistant prostate cancer. PLoS One 2014;9:e111201.
[32] Xu H, Yu X, Qu S, Chen Y, Wang Z, Sui D. Protective effect of *Panax quinquefolium* 20(*S*)-protopanaxadiol saponins, isolated from *Panax quinquefolium*, on permanent focal cerebral ischemic injury in rats. Exp Ther Med 2014;7:165–70.
[33] Kuo LM, Kuo CY, Lin CY, Hung MF, Shen JJ, Hwang TL. Intracellular glutathione depletion by oridonin leads to apoptosis in hepatic stellate cells. Molecules 2014;19:3327–44.
[34] Liu JJ, Huang RW, Lin DJ, Peng J, Wu XY, Lin Q, Pan XL, Song YQ, Zhang MH, Hou M, et al. Expression of survivin and bax/bcl-2 in peroxisome proliferator activated receptor-gamma ligands induces apoptosis on human myeloid leukemia cells in vitro. Annals Oncol 2005;16:455–9.
[35] Walsh JG, Cullen SP, Sheridan C, Lüthi AU, Gerner C, Martin SJ. Executioner caspase-3 and caspase-7 are functionally distinct proteases. Proc Natl Acad Sci U S A 2008;105:12815–9.
[36] Herceg C, Wang ZQ. Functions of poly(ADP-ribose) polymerase (PARP) in DNA repair, genomic integrity and cell death. Mutat Res 2001;477:97–110.

[37] Dong GZ, Jang EJ, Kang SH, Cho IJ, Park SD, Kim SC, Kim YW. Red ginseng abrogates oxidative stress via mitochondria protection mediated by LKB1–AMPK pathway. BMC Complement Altern Med 2013;13:64.
[38] Cai L, Hu K, Lin L, Ai Q, Ge P, Liu Y, Dai J, Ye B, Zhang L. AMPK dependent protective effects of metformin on tumor necrosis factor-induced apoptotic liver injury. Biochem Biophys Res Commun 2015;465:381–6.
[39] Zhang C, Liao Y, Li Q, Chen M, Zhao Q, Deng R, Wu C, Yang A, Guo Z, Wang D, et al. Recombinant adiponectin ameliorates liver ischemia reperfusion injury via activating the AMPK/eNOS pathway. PLoS One 2013;8:e66382.
[40] Cai X, Hu X, Cai B, Wang Q, Li Y, Tan X, Hu H, Chen X, Huang J, Cheng J, et al. Metformin suppresses hepatocellular carcinoma cell growth through induction of cell cycle G1/G0 phase arrest and p21CIP and p27KIP expression and downregulation of cyclin D1 in vitro and in vivo. Oncol Rep 2013;30:2449–57.
[41] Lee CW, Wong LL, Tse EY, Liu HF, Leong VY, Lee JM, Hardie DG, Ng IO, Ching YP. AMPK promotes p53 acetylation via phosphorylation and inactivation of SIRT1 in liver cancer cells. Cancer Res 2012;72:4394–404.
[42] Lian N, Jin H, Zhang F, Wu L, Shao J, Lu Y, Zheng S. Curcumin inhibits aerobic glycolysis in hepatic stellate cells associated with activation of adenosine monophosphate-activated protein kinase. IUBMB Life 2016;68:589–96.
[43] Zhai X, Qiao H, Guan W, Li Z, Cheng Y, Jia X, Zhou Y. Curcumin regulates peroxisome proliferator-activated receptor-γ coactivator-1α expression by AMPK pathway in hepatic stellate cells in vitro. Eur J Pharmacol 2015;746:56–62.
[44] Wullschleger S, Loewith R, Hall MN. TOR signaling in growth and metabolism. Cell 2006;124:471–84.
[45] Shaw RJ. LKB1 and AMP-activated protein kinase control of mTOR signalling and growth. Acta Physiol 2009;196:65–80.
[46] Gwinn DM, Shackelford DB, Egan DF, Mihaylova MM, Mery A, Vasquez DS, Turk BE, Shaw RJ. AMPK phosphorylation of raptor mediates a metabolic checkpoint. Mol Cell 2008;30:214–26.
[47] Djouder N, Tuerk RD, Suter M, Salvioni P, Thali RF, Scholz R, Vaahtomeri K, Auchli Y, Rechsteiner H, Brunisholz RA, et al. PKA phosphorylates and inactivates AMPKalpha to promote efficient lipolysis. EMBO J 2010;29:469–81.
[48] Kim SJ, Yuan HD, Chung SH. Ginsenoside Rg1 suppresses hepatic glucose production via AMP-activated protein kinase in HepG2 cells. Biol Pharm Bull 2010;33:325–8.
[49] Hien TT, Kim ND, Pokharel YR, Oh SJ, Lee MY, Kang KW. Ginsenoside Rg3 increases nitric oxide production via increases in phosphorylation and expression of endothelial nitric oxide synthase: essential roles of estrogen receptor-dependent PI3-kinase and AMP-activated protein kinase. Toxicol Appl Pharmacol 2010;246:171–83.
[50] Kim DY, Park MW, Yuan HD, Lee HJ, Kim SH, Chung SH. Compound K induces apoptosis via CAMK-IV/AMPK pathways in HT-29 colon cancer cells. J Agric Food Chem 2009;57:10573–8.